Zeeman ratchets: pure spin current generation in mesoscopic conductors with non-uniform magnetic fields

2007 New J. Phys. 9 401

(http://iopscience.iop.org/1367-2630/9/11/401)

New Journal of Physics
The open–access journal for physics

Zeeman ratchets: pure spin current generation in mesoscopic conductors with non-uniform magnetic fields

Matthias Scheid[1,3], **Dario Bercioux**[1,2] **and Klaus Richter**[1]

[1] Institut für Theoretische Physik, Universität Regensburg, D-93040 Regensburg, Germany

[2] Physikalisches Institut, Albert-Ludwigs-Universität, D-79104 Freiburg, Germany

E-mail: Matthias.Scheid@physik.uni-regensburg.de and Dario.Bercioux@physik.uni-freiburg.de

New Journal of Physics **9** (2007) 401

Received 16 July 2007

Published 6 November 2007

Online at http://www.njp.org/

doi:10.1088/1367-2630/9/11/401

Abstract. We consider the possibility to employ a quantum wire realized in a two-dimensional electron gas (2DEG) as a spin ratchet. We show that a net spin current without accompanying net charge transport can be induced in the nonlinear regime by an unbiased external driving via an ac voltage applied between the contacts at the ends of the quantum wire. To achieve this, we make use of the coupling of the electron spin to inhomogeneous magnetic fields created by ferromagnetic stripes patterned on the semiconductor heterostructure that harbors the 2DEG. Using recursive Green function techniques, we numerically study two different set-ups, consisting of one and two ferromagnetic stripes, respectively.

[3] Author to whom any correspondence should be addressed.

PII: S1367-2630(07)55257-2

Contents

1. Introduction

Spintronics as an emerging field of physics has attracted considerable attention in recent years and has developed into various inter-related branches covered in this focus issue. Spintronics is devoted to employing the spin degree of freedom for information storage and as another means for extending the functionality of electronic systems. Semiconductor spintronics, as one subfield, is guided by the idea of combining concepts of spin electronics with the established techniques and advantages of semiconductor physics and nanostructures. Up to now, their properties used mainly rely on the charge degree of freedom alone. Many ideas for employing spin-polarized currents have been put forward since the seminal proposal by Datta and Das for a spin transistor [1] based on spin precession controlled by an external electric field through spin–orbit (SO) coupling [2]. These proposals usually require spin injection, more generally, the creation of spin-polarized particles in these materials. Spin injection from a ferromagnetic metal source into semiconductors is hindered by a fundamental obstacle originating from the conductivity mismatch between these materials [3]. Though this problem may be partially circumvented, for instance at low temperatures by tailoring dilute-magnetic-semiconductor/semiconductor interfaces [4, 5] enabling considerable spin-polarization ratios of the order of 90% [4], building all-semiconductor sources of spin-polarized electrons is still a challenge.

Alternatively, several techniques to intrinsically create spin currents in non-magnetic systems have been put forward: non-equilibrium spin-polarized currents have been created in two-dimensional electron gases (2DEGs) realized in zinc-blende-based heterostructures by means of optical pumping [6]. The irradiation of the 2DEG with circularly polarized light results in a spin photocurrent caused by the non-uniform distribution of the photoexcited carriers in **k**-space owing to optical selection rules and energy and momentum conservation. The recently proposed intrinsic spin-Hall effect in *p*-doped [7] bulk systems and in 2DEGs [8] offers the principle possibility for spin current generation and manipulation in high mobility

semiconducting systems. The combined effect of an applied electric field and the torque induced by SO coupling tilts the spins out of the 2DEG plane. This leads to spin accumulation at both sides of the sample in the direction perpendicular to the applied electric field. Spin-Hall effects have been observed experimentally both in semiconducting systems by optical detection techniques [9]–[11] and in metallic systems with an all-electrical set-up [12, 13].

In the context of mesoscopic physics, further concepts such as adiabatic spin pumping [14]–[16] and coherent spin ratchets [17, 18] have been proposed for generating spin-polarized currents. This can be achieved by exploiting the magnetic properties of the semiconducting material, i.e. intrinsic SO interaction or the Zeeman coupling to external magnetic fields.

Adiabatic quantum pumping involves the generation of a directed current in the absence of a bias voltage by periodic modulations of two or more system parameters, such as, e.g. the shape of the system or a magnetic field [19]. The spin analog of the charge quantum pump can be achieved through an external magnetic field [15] or SO interaction [16] in order to filter the pumped current. For the case of an external magnetic field, it has been experimentally confirmed that under specific circumstances a spin current can be extracted from spin-dependent conductance fluctuations without accompanying net charge flow [20].

Ratchets [21] are generally systems with broken inversion (left/right) symmetry that generate directed net (particle) currents upon external ac driving in the absence of a net (time-averaged) bias potential. Thereby they have much in common with current rectifiers, though there are differences, in particular in the dissipative case [21]. The theoretical concept of ratchets, originally introduced for classical dynamics, was later extended to the quantum dissipative regime [22]. As a main feature, which distinguishes them also from rectifiers in the usual sense, quantum ratchets exhibit current reversal upon changing, e.g. the temperature or energy. Such quantum ratchets were experimentally realized in semiconductor heterostructures by demonstrating directed charge flow in a chain of asymmetric ballistic electron cavities in the low-temperature regime, where the dynamics was close to coherent [23]. In this and further experimental investigations [24] also the charge current reversal phenomenon has been demonstrated.

Very recently, we have proposed the generalization of the ratchet mechanism, extensively explored for particle motion, to generate directed spin currents. Spin ratchets require a coupling to the electron spin which, e.g. can be provided via SO interaction or external (non-uniform) magnetic fields. In Scheid *et al* [17], *spin–orbit ratchets* have been considered in the coherent regime. There, a proof of principle for a net ratchet spin current (in the absence of an average charge current) has been given and confirmed by numerical calculations for experimentally accessible parameters for GaAs-based heterostructures.

In the present paper, we further investigate the possibility of employing *Zeeman ratchets* for spin current generation, i.e. by considering mesoscopic conductors with a spatially varying Zeeman term and subject to an ac bias. In the simplest case of one-dimensional (1D) motion, and assuming preserved spin states, spin-up and spin-down electrons will experience a Zeeman term, $\pm(g^*/2)\,\mu_{\mathrm{B}}B(x)$, where $B(x)$ is the external non-uniform magnetic field, g^* the effective gyroscopic factor and μ_{B} the Bohr magneton. If $B(x) \neq B(-x)$, then the different spin species experience opposite asymmetric Zeeman ratchet potentials. In close analogy to the particle ratchet mechanism described above, the different spins are expected to be predominantly driven into opposite directions upon external driving, resulting in a spin-polarized current. This mechanism has been studied and confirmed by Scheid *et al* [18].

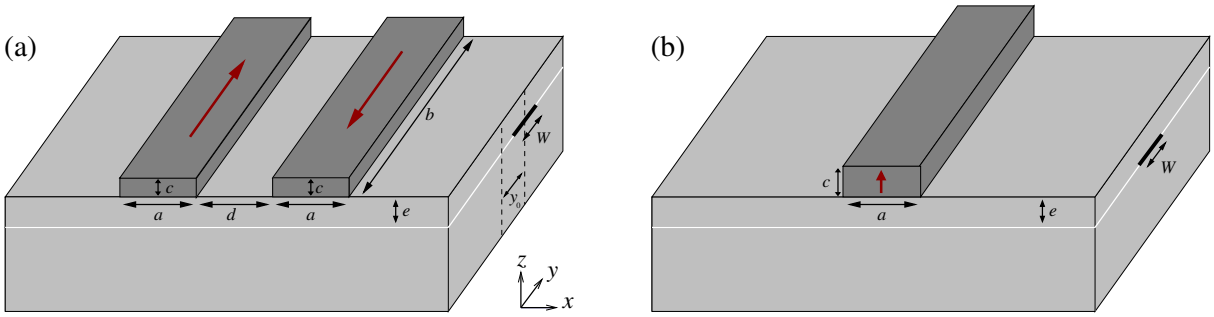

Figure 1. Ferromagnetic stripes (magnetization direction given by red arrows) on top of a semiconductor heterostructure that harbors a 2DEG (indicated by white lines) containing a quantum wire (black) of width W. (a) Set-up A: two stripes with antiparallel in-plane magnetization, see section 3; (b) set-up B: one stripe with out-of-plane magnetization, see section 4.

In the present work, we relax both assumptions of 1D motion [25] and conserved spin directions, e.g. the notion of two independent spin species and explicitly include spin-flip effects. Moreover, we work out how such spin-flip processes can be invoked to engineer and tune ratchet spin conductances. To this end, we consider spin ratchet effects of a system consisting of a 2D quantum wire embedded in 2DEG and subject to an ac bias in between two ohmic contacts. The non-uniform B-field is created by the magnetic fringe fields of ferromagnetic stripes patterned on the semiconductor heterostructure [26].

This paper is organized as follows: in section 2, we introduce the model for the spin ratchet. We thereby specify the driving of the ratchet and the evaluation of the net charge and spin currents. In section 3, we study transport through the quantum wire subject to the magnetic fringe fields of two ferromagnetic stripes with antiparallel magnetization perpendicular to the quantum wire in the plane of the 2DEG. This configuration (set-up A in figure 1(a)) allows us to study the transition from decoupled to strongly coupled spin states and its implications on transport and thus also on the ratchet currents. In section 4, we then investigate the conductor subject to the fringe field of a single ferromagnetic stripe magnetized perpendicular to the plane of the 2DEG (set-up B in figure 1(b)). Using symmetry arguments and numerical calculations, we demonstrate that the two set-ups introduced in sections 3 and 4 act as spin ratchets. After summarizing in section 5, we close the paper with an appendix on the general derivation of an expression for the spin current within the framework of the multi-terminal Landauer–Büttiker formalism and a second appendix including the derivation of symmetry relations for the transport properties at finite applied bias.

2. Model and formalism

We consider a quantum wire in the x-direction embedded in a 2DEG in the (x, y)-plane. The system is subject to a non-uniform magnetic field $\vec{B}(x, y)$, due to the fringe fields of ferromagnetic stripes patterned on top of the 2DEG (see figure 1). Their deposition on a semiconductor heterostructure can be accomplished with electron beam lithography and lift-off techniques [27, 28]. Near-surface 2DEGs can be fabricated to lie only a few tens of

nanometres beneath the surface [28], thereby achieving magnetic field values of up to 0.5 T with thin ferromagnetic films [29]. The magnetic fringe field of a ferromagnet with homogeneous magnetization $\vec{M}$ is given by [30]

$$\vec{B}(\vec{r}) = -\frac{\mu_0}{4\pi}\vec{\nabla}\oint_S \mathrm{d}a' \, \frac{\vec{M}\times\hat{u}(\vec{r}')}{|\vec{r}-\vec{r}'|}, \tag{2.1}$$

where the integration runs over the surface S of the ferromagnetic stripe, and $\hat{u}(\vec{r}')$ is the unit vector normal to the surface of the stripe at position $\vec{r}'$. Accordingly, the corresponding vector potential in the Coulomb gauge, $\vec{\nabla}\cdot\vec{A}=0$, is given by [30]

$$\vec{A}(\vec{r}) = \frac{\mu_0}{4\pi}\oint_S \mathrm{d}a' \frac{\vec{M}\times\hat{u}(\vec{r}')}{|\vec{r}-\vec{r}'|}. \tag{2.2}$$

We model the wire, where electron transport is assumed to be phase coherent, by the single-particle Hamiltonian

$$\hat{\mathcal{H}}_0 = \frac{\Pi_x(x,y)^2+\Pi_y(x,y)^2}{2m^*} + \frac{g^*\mu_\mathrm{B}}{2}\vec{B}(x,y)\cdot\vec{\sigma} + V(y), \tag{2.3}$$

where g^* is the effective gyroscopic factor, m^* the effective electron mass, μ_B the Bohr magneton and $\vec{\sigma}$ the vector of the Pauli matrices. The term $V(y)$ denotes the lateral confining potential defining the quantum wire. Orbital effects due to the magnetic field are accounted for by the vector potential $\vec{A}(x,y)$ in $\vec{\Pi}(x,y)=\vec{p}-\mathrm{e}\vec{A}(x,y)$. Spin effects in transport through the wire enter via the Zeeman term $(g^*\mu_\mathrm{B}/2)\vec{B}\cdot\vec{\sigma}$ coupling the spin degree of freedom to the external magnetic field. For a proper treatment of the spin evolution, the inclusion of the full magnetic field profile is mandatory [31]; disregarding [32] one of the magnetic field components B_i may lead to an oversimplification of the problem.

To obtain a significant spin ratchet effect materials with a large g^* factor are most suitable. In this respect dilute magnetic semiconductors (DMS) represent a promising class of materials. Recent measurements have shown values of $g^*>100$ [33], where in addition to the intrinsic g-factor, an additional contribution to g^* appears, owing to exchange coupling among the electron spins and the magnetic ions present in the DMS [34]. These materials with a large g^* factor can also exhibit large SO coupling values. The working principle of a spin ratchet based on SO coupling has been already investigated in Scheid *et al* [17]. As one result of this study a spin-ratchet effect can only occur if there exists the possibility to mix different transverse channels of the wire. This can only happen when more than one open channel is taking part in the transport and electrostatic barriers induce this mixing of different bands. As we will show below, the spin-ratchet effect created by the setup presented in this paper does not rely on this condition and is already present when only the first conducting channel is opened. Due to this fact and the absence of any electrostatic barriers responsible for the mixing of different subbands, we disregard here the SO coupling and focus on the effects due to the presence of the magnetic stripes.

In the present work where we consider disorder-free ballistic motion, we refer to nonmagnetic high-mobility semiconductors. To be definite, we chose throughout the paper parameters for InAs 2DEGs with typical values of $m^*=0.024m_0$ [35], where m_0 is the free electron mass, and $|g^*|=15$. InAs is well suited due to its large g^* factor and the property that InAs 2DEGs can be fabricated close to the surface where the magnetic stripes are located. We assume that the stripes possess a magnetization $\mu_0 M = 3\mathrm{T}$.

The charge current I_C through the wire is evaluated within the Landauer approach. For coherent transport in a two-terminal device the current can be expressed as

$$I_C = -\frac{e}{h}\int_0^\infty dE\,\left[f(E;\mu_L) - f(E;\mu_R)\right]T(E) \tag{2.4}$$

in terms of the quantum probability $T(E)$ for electrons with energy E to be transmitted from the lead at higher to the lead at lower potential. In equation (2.4), $f(E;\mu_{L/R})$ is the Fermi function for the left/right lead with chemical potential $\mu_{L/R}$.

The spin current $I_S(x)$ passing a cross-section ($x = \text{const.}$) is given, for a wavefunction $\Psi(x, y)$, by

$$I_S(x) = \int dy\,\Psi^*(x, y)\hat{J}_S\Psi(x, y).$$

Here, we use the most common definition [36] of the spin current operator $\hat{J}_S$ which, with respect to an arbitrary quantization axis $\hat{u}$, reads

$$\hat{J}_S = \frac{\hbar}{2}\frac{\hbar}{2m^*i}\left(\vec{\sigma}\cdot\hat{u}\right)\left(\frac{\overrightarrow{\partial}}{\partial x} - \frac{\overleftarrow{\partial}}{\partial x}\right), \tag{2.5}$$

inside the leads. The partial derivatives in (2.5) act on expressions to their right and left (indicated by the arrows).

Contrary to the charge current that obeys a continuity equation, the spin current can take different values if evaluated in the left or in the right lead. This usually happens in systems where the Hamiltonian does not commute with the Pauli matrices $\vec{\sigma}$ giving rise to a torque inside the scattering region [37], which can change the spin state of the electrons. For this reason we will explicitly label the lead, where we compute the spin current. Although there is some ambiguity in the choice of the spin current operator [38], here we evaluate the spin current inside the magnetic field free leads, where a torque term in the continuity equation for spin is absent. Therefore, the spin current inside the leads is a well-defined quantity, which can be measured in principle. As derived in appendix A (equation A.9) the corresponding spin current in the right lead reads

$$I_S = \frac{1}{4\pi}\int_0^\infty dE\,\left[f(E;\mu_L) - f(E;\mu_R)\right]T_S(E), \tag{2.6}$$

with the spin transmission probability defined as

$$T_S(E) = \sum_{\sigma=\pm1}\left[T_{+,\sigma}(E) - T_{-,\sigma}(E)\right]. \tag{2.7}$$

Here $T_{\sigma',\sigma}$ is the probability for an electron with initial spin state σ to be transmitted from the left lead into the spin state σ' inside the right lead, see equation (A.7) in appendix A. To obtain the corresponding spin current in the left lead one has to replace $T_{\sigma',\sigma}(E)$ in equation (2.7) by the corresponding probabilities $T'_{\sigma',\sigma}(E)$ for transmission from the right to the left lead.

Ordinary particle ratchets give rise to a net drift motion of particles in one preferential direction upon ac driving without net bias (rocking ratchet). Below we will generalize this concept to induce spin-dependent ratchet currents correspondingly. The ac driving can be considered as adiabatic, since the timescales for the variation of an external bias potential are long compared to the relevant timescales for charge transmission through the device. For a proof of principle, we assume an adiabatic unbiased square-wave driving with period t_0.

The system is periodically switched between two rocking conditions, labeled by bias $\pm U_0$ ($U_0 > 0$). The electro-chemical potential $\mu_{L/R}$ of the left/right reservoir is changed periodically in time according to

$$\mu_{L/R}(t) = \begin{cases} \varepsilon_F \pm U_0/2, & \text{for} \quad 0 \leqslant t < t_0/2, \\ \varepsilon_F \mp U_0/2, & \text{for} \quad t_0/2 \leqslant t < t_0, \end{cases} \tag{2.8}$$

i.e. $\mu_{L/R}(t) = \mu_{L/R}(t + t_0)$. In the adiabatic limit considered, the system is assumed to be in a steady state between the switching events. Then the ratchet charge and spin currents inside the wire are obtained upon averaging equations (2.4) and (2.6) between the two rocking situations

$$\langle I_C(\varepsilon_F, U_0)\rangle = \tfrac{1}{2}\left[I_C(\varepsilon_F, +U_0) + I_C(\varepsilon_F, -U_0)\right] = -\tfrac{e}{2h}\int_0^\infty \mathrm{d}E\, \Delta f(E; \varepsilon_F, U_0)\Delta T(E; U_0)\,, \tag{2.9a}$$

$$\langle I_S(\varepsilon_F, U_0)\rangle = \tfrac{1}{2}\left[I_S(\varepsilon_F, +U_0) + I_S(\varepsilon_F, -U_0)\right] = \tfrac{1}{8\pi}\int_0^\infty \mathrm{d}E\, \Delta f(E; \varepsilon_F, U_0)\Delta T_S(E; U_0)\,, \tag{2.9b}$$

where

$$\begin{aligned} \Delta f(E; \varepsilon_F, U_0) &= f(E; \varepsilon_F + U_0/2) - f(E; \varepsilon_F - U_0/2), \\ \Delta T(E; U_0) &= T(E; +U_0) - T(E; -U_0), \\ \Delta T_S(E; U_0) &= T_S(E; +U_0) - T_S(E; -U_0). \end{aligned} \tag{2.10}$$

An extension to an adiabatic harmonic driving is straightforward.

In linear response, the ratchet spin current $\langle I_S\rangle$, equation (2.9*b*), vanishes because $\Delta T_S(E; U_0 = 0) = 0$, see equation (2.10). Hence, we must consider the nonlinear regime to obtain a finite net spin current. Since we consider nonlinear transport ignoring inelastic processes, we can write the currents equations (2.4) and (2.6) as energy integrals over the transmission. To model a finite voltage drop across the two leads, we add the term

$$\hat{\mathcal{H}}_U = U g(x, y; U), \tag{2.11}$$

to the Hamiltonian (2.3), where for the square wave driving considered here, U takes the values $\pm U_0$ respectively. Here the function $g(x, y; U)$ describes the spatial distribution of the electrostatic potential inside the mesoscopic system and is generally obtained through a self-consistent solution of the many-particle Schrödinger equation and the Poisson equation [39, 40]. However, here we employ heuristic models for $g(x, y; U)$, assuming that the voltage primarily drops in regions, where the magnetic field strongly varies spatially. This model is based on the fact that the corresponding Zeeman term acts as an effective potential barrier, and takes into account that a more rapid potential variation leads to enhanced wave reflection and hence to a steeper local voltage drop [41] (details will be given in the following sections).

In order to numerically evaluate the transport properties of the system, the stationary Schrödinger equation $(\hat{\mathcal{H}} - E)\Phi(\vec{r}) = 0$ is discretized on a square lattice, yielding a tight-binding representation of $\hat{\mathcal{H}}$. This is then used to calculate the elements of the scattering matrix of the system via lattice Green's functions and a recursive Green's function algorithm [42].

3. Set-up A: two ferromagnetic stripes with longitudinal magnitization

In this section, we investigate the spin-dependent transport properties (and thereby also the operability as a ratchet) of a quantum wire in the plane of the 2DEG subject to the magnetic field of two stripes with opposite, longitudinal in-plane magnetizations, $\vec{M} = \pm M\hat{y}$, arranged perpendicular to the wire. This set-up A is shown in figure 1(a). The Hamiltonian of the system

is given by equation (2.3) with $A_y = 0$ (in the Coulomb gauge), i.e. $\Pi_y = p_y$. For the following analysis we chose a confinement potential $V(y)$ such that the wire of width W is displaced by a shift y_0 with respect to the symmetric configuration, see figure 1.

For sufficiently narrow wires ($W \ll b$) and small displacement ($y_0 \ll b$), the energy scales of the magnetic field contributions to $\hat{\mathcal{H}}_0$ in equation (2.3) containing $\vec{B}$ and $\vec{A}$ are much smaller than differences between energy levels $E_m - E_n$ of different transversal modes $|m\rangle$ and $|n\rangle$. Therefore, transitions between different transversal modes are strongly suppressed, and we consider the case of only one open mode. Higher modes $|n\rangle$ mimic the behavior of the first mode up to an energy offset $E_n - E_1$.

Evaluating equation (2.1) for the combined magnetic field of two stripes centered around $(x = 0, y = 0)$, set-up A, we obtain the following symmetry properties for the B-field components of this configuration:

$$B_x(x, -y, z) = -B_x(x, y, z), \tag{3.1a}$$

$$B_y(x, -y, z) = B_y(x, y, z), \tag{3.1b}$$

$$B_z(x, -y, z) = -B_z(x, y, z). \tag{3.1c}$$

In particular, equations (3.1*a*) and (3.1*c*) imply vanishing magnetic field components B_x and B_z for $y = 0$. Therefore, we use $\hat{y}$ as the spin quantization axis for the considerations below. Those symmetries also have an important implication for the spin dynamics of the system. For a confinement potential that is symmetric upon reflection at the (x, z)-plane, $V(-y) = V(y)$, as realized for a symmetric confinement centered around $y_0 = 0$, spin-up and spin-down eigenstates within the same transversal mode n are decoupled. The relevant matrix element $\langle n, \sigma | \vec{\sigma} \cdot \vec{B}(x, y) | n, -\sigma \rangle$, responsible for the spin mixing, vanishes,

$$\int_{-\infty}^{\infty} \mathrm{d}y \, |\chi_n(y)|^2 \left[B_z(x, y) - \mathrm{i}\sigma B_x(x, y) \right] = 0 \,, \tag{3.2}$$

since the integrand is an odd function of y due to equations (3.1*a*) and (3.1*c*) and the fact that transversal modes obey $\chi_n(-y) = (-1)^{n-1}\chi_n(y)$. However, for finite values of y_0, the coupling (3.2) does not vanish anymore, and spin flips can arise with a significant effect on electron transport, as we will demonstrate in the next section.

3.1. DC transport

Before evaluating the average charge current (2.9*a*) and spin ratchet current (2.9*b*), it is instructive to analyze the dc transport properties of set-up A. To this end we chose as realistic parameters for the geometry (see figure 1(a)) $W = 120\,\mathrm{nm}$, $a = 600\,\mathrm{nm}$, $b = 2\,\mu\mathrm{m}$ (thus $W/b = 0.06$), $c = 200\,\mathrm{nm}$, $d = 600\,\mathrm{nm}$ and $e = 100\,\mathrm{nm}$. For this parameter set and $y_0 \ll b$ the magnetic field component $B_y(x, y)$ is approximately constant in y-direction, i.e. $B_y(x, y) \approx B_y(x)$. It possesses a much larger maximum value than the other components B_x and B_z. In figure 2, we show the x-dependence of the overall magnetic fringe field of the two-stripe set-up A for fixed $y = 200\,\mathrm{nm}$.

Figure 3 shows the total transmission $T(E)$ in linear response ($U_0 \to 0$) for energies within the first transversal subband for different values of y_0. For $y_0 = 0$, the spin eigenstates decouple owing to equation (3.2). The energy where the first transversal mode opens is shifted to $E \approx E_1 + U_\mathrm{B}$ due to the Zeeman barrier of height $U_\mathrm{B} = g^* \mu_\mathrm{B} \max[B_y(x, y = 0)]/2$ present in

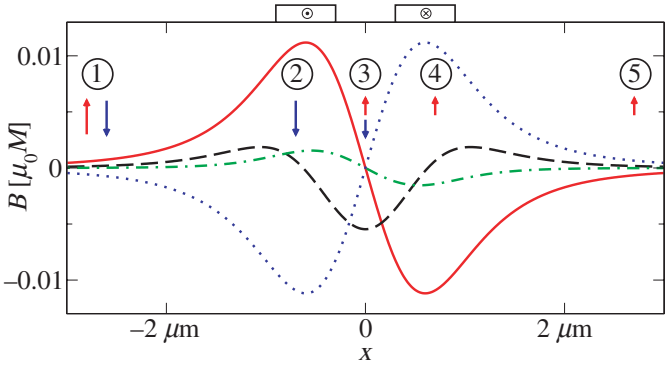

Figure 2. Magnetic field components B_x (dash-dotted green line), B_y (solid red), $-B_y$ (dotted blue) and B_z (dashed black) in the plane of the 2DEG at fixed $y = 200$ nm for set-up A, figure 1(a) and parameters given in the text.

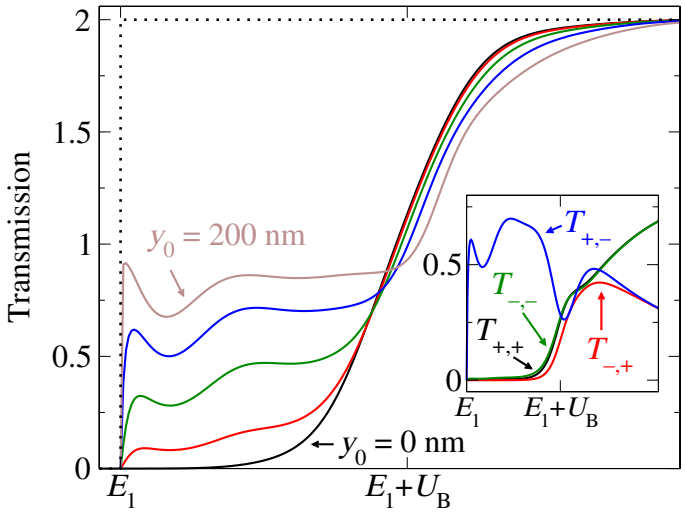

Figure 3. Total transmission $T(E)$ in linear response for values of $y_0 = 0$ nm to 200 nm in steps of 50 nm from bottom (black line) to top (brown line). The dotted black line indicates the transmission for $\vec{B} = 0$. Inset: spin-resolved transmission probabilities $T_{\sigma',\sigma}$, equation (A.7), for $y_0 = 100$ nm.

the wire. However, for increasing y_0 when spin flips can take place, an additional plateau builds up at energies $E_1 \leqslant E \leqslant E_1 + U_B$ approaching $T \approx 1$. In the inset of figure 3, the spin-resolved transmission probabilities $T_{\sigma',\sigma}$ are depicted for $y_0 = 100$ nm. We identify $T_{+,-}(E)$ as the sole contribution to the total transmission $T(E)$ for $E_1 \leqslant E \leqslant E_1 + U_B$. Thus the appearance of the additional plateau is a consequence of the mixing of the spin states. For energies well above the barrier both, spin-up and spin-down electrons are fully transmitted.

The main features in the numerically calculated transmission in figure 3 can be understood using a heuristic model. It is based on the fact that in the region close to $x = 0$ (see figure 2) spin flips predominantly take place, since $B_y(x, y) = 0$ vanishes at $x = 0$, and spin-up and spin-down states of the same transversal mode are nearly energy degenerate.

In the following we consider stepwise (positions labeled in figure 2) the spin evolution along the wire for unpolarized electrons entering the system with energy $E_1 \leqslant E \leqslant E_1 + U_B$:

1. Unpolarized electrons (equal number of spin-up and spin-down particles) are injected from the left reservoir.
2. Spin-up electrons are completely reflected at the Zeeman barrier (indicated by the solid red line), while spin-down electrons experience a potential valley (blue dotted line) and can pass.
3. A fraction of the spins is flipped from down to up due to a finite $B_z(x)$ close to $x = 0$.
4. Spin-down electrons are completely reflected while spin-up electrons pass.
5. Only spin-down electrons from the left lead reach the right lead, after undergoing a spin flip.

Hence, this mechanism leads to $T_{+,+} = T_{-,+} = T_{-,-} = 0$ and $T_{+,-} \neq 0$. Although the model can explain the basic features of the transmission curves shown in figure 3 fairly well, it cannot account for the details in the functional dependence of $T(E)$ for energies below the barrier which reflects further quantum effects present, e.g. resonant tunneling processes. An analysis of the spin-resolved transmission probabilities in the opposite rocking situation, $\mu_L < \mu_R$, where electrons flow from right to left, shows that transmitted particles are oppositely spin-polarized compared with the former case. Correspondingly, $T'_{-,+}$ is the only non-zero component of the spin-resolved transmission for energies $E \leqslant E \leqslant E_1 + U_B$.

The above analysis demonstrates that the magnetic field components perpendicular to the dominant one, even if they are small, can significantly alter the transport properties of the system. In the present case, disregarding B_x and B_z would have resulted in a vanishing transmission for $E < E_1 + U_B$.

3.2. AC transport

We now investigate the rectification properties of set-up A upon applying the ac driving given in equation (2.8). We first specify how we obtain the drop of the electrostatic potential $g(x, y; U)$ across the system for a finite applied bias. Based on a heuristic model used by Linke *et al* [24], we assume that $(\partial g(x)/\partial x) \propto |(\partial/\partial x) B_y(x, y = 0)|$ in the central scattering region, $-L/2 < x < L/2$, yielding

$$g(x) = \frac{1}{2} - \frac{\int_{-L/2}^{x} \mathrm{d}x |(\partial/\partial x) B_y(x, y = 0)|}{\int_{-L/2}^{L/2} \mathrm{d}x |(\partial/\partial x) B_y(x, y = 0)|}, \tag{3.3}$$

while we fix $g(x)$ to $\pm 1/2$ inside the left (right) lead. For the full system Hamiltonian $\hat{\mathcal{H}} = \hat{\mathcal{H}}_0 + \hat{\mathcal{H}}_U$, equations (2.3) and (2.11), at finite bias U_0 we evaluate the expressions (2.9*a*) and (2.9*b*) for the average charge and spin currents. If orbital effects due to the perpendicular magnetic field B_z are negligible, i.e. $A_y \simeq 0$, the total Hamiltonian $\hat{\mathcal{H}}$ is invariant under the symmetry operation $\hat{\mathcal{P}} = \hat{R}_x \hat{R}_U \sigma_z$. Then, as shown in appendix B, the relation (B.4) between S-matrix elements holds true. Squaring S-matrix elements in equation (B.4) and summing over channels $(n\sigma) \in L$ and $(n'\sigma') \in R$ yields $T(E; \pm U_0) = T'(E; \mp U_0)$. This relation, together with the relation $T'(E; \mp U_0) = T(E; \mp U_0)$ due to unitarity of the S-matrix, leads to $\langle I_C \rangle = 0$. A vanishing average charge current is in line with symmetry considerations for charge ratchets and coincides with a numerical analysis for the parameters used here.

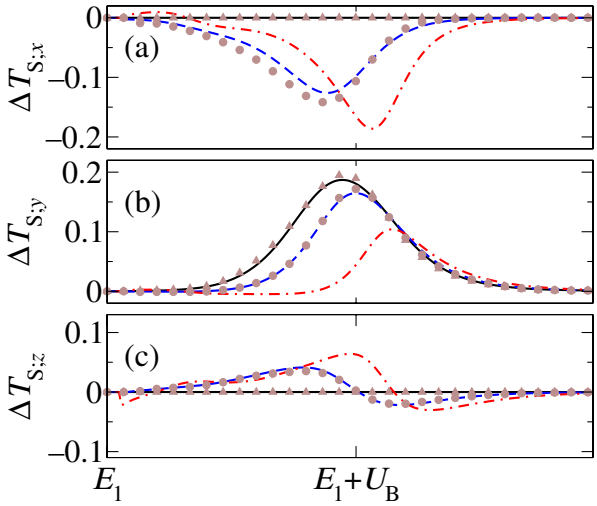

Figure 4. Ratchet spin transmission ΔT_S for spin quantization axes $\hat{x}$ (a), $\hat{y}$ (b) and $\hat{z}$ (c) as a function of the injection energy for displacement $y_0 = 0$ (solid black line), 100 (dashed blue) and 200 nm (dash-dotted red) for bias potential $U_0 = 0.1U_B$ and $g(x)$ specified in equation (3.3). For comparison, ΔT_S at $y_0 = 0$ (brown triangles) and 100 nm (brown circles) is shown for a linear voltage drop $\tilde{g}(x) = -x/L$ across the central scattering region with bias potential $\tilde{U}_0 \approx 2.3U_0$.

However, on the other hand, the symmetry considerations imply that the average spin current can take finite values. To confirm this numerically and to get an idea of its magnitude, we calculate the ratchet spin current in the right lead according to equation (2.9*b*). Figure 4 shows the differences in spin transmissions, $\Delta T_S(E)$, for the two rocking situations as a function of energy for moderate finite applied bias voltage $U_0 = 0.1U_B$. For $y_0 = 0$, where transitions between spin-up and spin-down states of the same transversal subband are absent, the system is comparable to the devices studied by Scheid *et al* [18]. There, it was shown, in analogy to the case of charge rectification [43], that for conserved spin eigenstates the ratchet effect stems from different maximum values $\Delta_{max}(U_0)$ of the effective potential landscape in the two rocking situations,

$$\Delta_{max}(U_0) = \max[U_{eff,\sigma}(x, +U_0)] - \max[U_{eff,\sigma}(x, -U_0)], \tag{3.4}$$

with

$$U_{eff,\sigma}(x, \pm U_0) = \pm U_0 g(x) + (\sigma/2)\mu_B g^* B_y(x, y = 0). \tag{3.5}$$

This mechanism explains the rectification related to $\Delta T_{S;\hat{y}}(E; y_0 = 0)$ (solid black line in figure 4(b)) and its functional dependence for $y_0 = 0$. There spin flips are absent and hence $T_{+,-} = T_{-,+} = 0$. For increasing y_0 the magnitude of $\Delta T_{S;\hat{y}}(E)$ decreases, while, at the same time, $\Delta T_{S;\hat{x}}(E)$ and $\Delta T_{S;\hat{z}}(E)$ grow and take finite values. Thus, we can summarize that the ratchet effect survives in the presence of mixing of different spin states. However, as apparent from figure 4, the vector of spin polarization is no longer aligned along $\hat{y}$ for finite y_0.

We further study how sensitively the observed effect depends on the particular form of the voltage drop $g(x)$. To this end in figure 4, we additionally show ΔT_S for a linear voltage drop model $\tilde{g}(x) = -x/L$ (brown circles/triangles) inside the central region

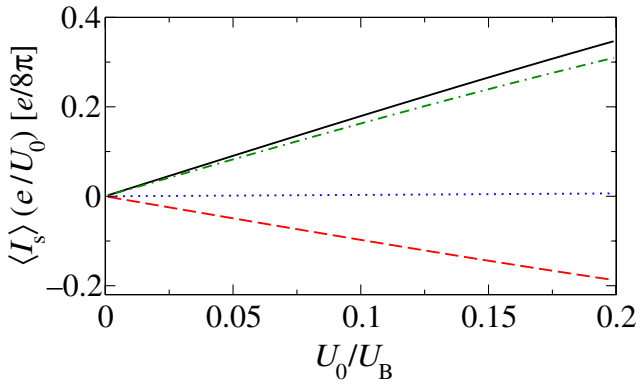

Figure 5. Bias voltage dependence of the ratchet spin conductance $\langle I_{S;\hat{u}} \rangle (e/U_0)$ at zero temperature, $k_B T = 0$, for a Fermi energy $\varepsilon_F = E_1 + U_B$. Results are shown for $y_0 = 0$ and polarization axis $\hat{u} = \hat{y}$ (black solid line), and for $y_0 = 100$ nm and $\hat{u} = \hat{x}$ (red dashed line), $\hat{y}$ (green dash-dotted line) and $\hat{z}$ (blue dotted line).

$(-L/2 < x < L/2)$, where the bias voltage $\tilde{U}_0$ was chosen such that the maximum value of the respective effective potential (3.5) was the same for both voltage drop models: $\max[U_{\mathrm{eff},\sigma}(x, \pm U_0)] = \max[\tilde{U}_{\mathrm{eff},\sigma}(x, \pm \tilde{U}_0)]$. Comparing $\Delta T_S(E; y_0)$ for $\tilde{g}(x)$ at $y_0 = 0$ (brown triangles) and 100 nm (brown circles) with the respective function $\Delta T_S(E; y_0)$ for $g(x)$, we observe no significant difference in their functional dependence on E, although the magnitude of the overall bias is different for both models ($\tilde{U}_0 \approx 2.3 U_0$ for the curves presented in figure 4). Therefore, we can state that $\Delta T_S(E; y_0)$ rather depends on the difference (3.4) in the maximum values of the effective potential than the actual distribution of the electrostatic potential in the mesoscopic conductor. A study of ΔT_S in the other lead shows very similar results to the ones presented in figure 4.

In figure 5, we finally display the ratchet spin conductance $\langle I_S(\varepsilon_F, U_0) \rangle (e/U_0)$, equation (2.9*b*), which shows a nearly linear dependence on the bias voltage U_0, i.e. $\Delta T_S(E; y_0) \propto U_0$. This is in line with the above analysis showing that $\Delta T_S(E; y_0) \propto \Delta_{\max}(U_0)$ and $\Delta_{\max}(U_0) \propto U_0$.

4. Set-up B: a single ferromagnetic stripe with transverse magnetization

In the following, we investigate the possibility of generating a spin ratchet effect using the magnetic field profile of a single stripe magnetized in the (x,z)-plane as shown in figure 1(b). For $b \gg W$, the evaluation of equations (2.1) and (2.2) for a magnetization $\vec{M} = M_x \hat{x} + M_z \hat{z}$ yields

$$\vec{B}(\vec{r}) = \begin{pmatrix} B_x(x,z) \\ 0 \\ B_z(x,z) \end{pmatrix}, \qquad \vec{A}(\vec{r}) = \begin{pmatrix} 0 \\ A_y(x,z) \\ 0 \end{pmatrix}.$$

The Hamiltonian of this system then reads

$$\hat{\mathcal{H}}_0 = \frac{p_x^2 + \Pi_y(x)^2}{2m^*} + g^* \frac{\mu_B}{2} \Big[B_x(x)\sigma_x + B_z(x)\sigma_z \Big] + V(y).$$

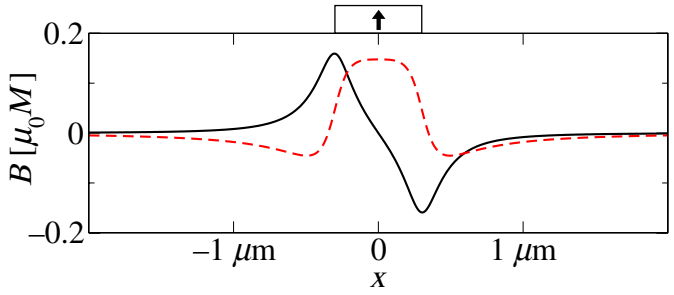

Figure 6. Magnetic field components $B_x(x)$ (solid black line) and $B_z(x)$ (dashed red line) in the plane of the 2DEG produced by a ferromagnetic stripe ($a = 600\,\text{nm}$, $b \to \infty$, $c = 200\,\text{nm}$, $e = 100\,\text{nm}$, see figure 1(b)) with magnetization $\vec{M} = M\hat{z}$.

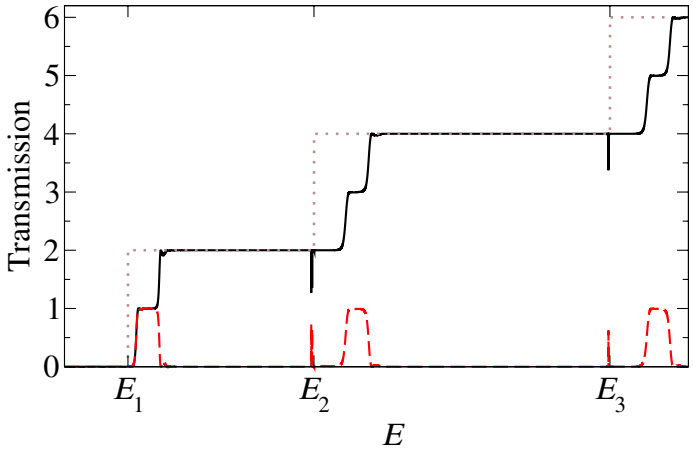

Figure 7. Total transmission $T(E)$ (solid black line) and absolute value of the spin transmission $|T_S|$ (dashed red line) as a function of energy for a wire underneath a single ferromagnetic stripe, see figure 1(b) and text. For comparison, the dotted brown staircase function shows the transmission in the absence of a magnetic field.

The 2DEG is located $e = 100\,\text{nm}$ below the surface of the semiconductor heterostructure (see figure 1(b)). The extension of the stripe in x-direction is chosen to be $a = 600\,\text{nm}$, infinite in y-direction and $c = 200\,\text{nm}$ in z-direction. For the analysis below, we chose a stripe magnetization $\vec{M} = M\hat{z}$. The corresponding magnetic field in the plane of the 2DEG is depicted in figure 6. Results comparable to those presented below are obtained for a stripe magnetized in x-direction.

4.1. DC transport

In figure 7, we show the total transmission $T(E)$ for a quantum wire of width $\text{W} = 120\,\text{nm}$ subject to the B-field, figure 6, in linear response ($U_0 \to 0$). In addition to the steps at even values of $T(E) \approx 2, 4, 6, \ldots$ due to the successive opening of the transversal modes at energies $E_n = [h^2\pi^2/(2m^*W^2)]n^2$, additional plateaus appear at odd values of $T(E) \approx 1, 3, 5, \ldots$ close

to the energies E_n. As in section 3, we can attribute these features to the lifted spin degeneracy due to the Zeeman field, since also the width of these plateaus corresponds to twice the absolute height of the Zeeman barrier $U_B = (g^*/2)\,\mu_B \max[|\vec{B}|]$ inside the wire.

In figure 7, we furthermore plot the absolute value of the spin transmission, $|T_S| = \sqrt{(T_{S;x})^2 + (T_{S;y})^2 + (T_{S;z})^2}$, which approaches unity at energies of the additional plateaus. A closer look at the spin- and mode-resolved transmission probabilities reveals that the transmission of the highest occupied transversal subband is completely spin polarized at the plateaus, while the lower modes are fully transmitting spin-up and spin-down particles. Similar results were reported by Zhai and Xu [31] for a stripe magnetized in the x-direction.

Apart from the spin effects due to the Zeeman term, the vector potential component A_y, affecting the orbital dynamics of the electrons due to the perpendicular magnetic field B_z, influences the electron transport. In a classical picture, B_z forces electrons to move on segments of cyclotron orbits in the plane of the 2DEG. Therefore, the kinetic energy in the direction of motion is reduced resulting in a shift of the energies where the transversal modes open towards higher values [44]. This is visible in figure 7, when comparing the total transmission with (solid black line) and without (dotted brown line) magnetic field.

4.2. AC transport

As for set-up A, we employ a heuristic model for the voltage drop inside the mesoscopic conductor, assuming $\partial g(x)/\partial x \propto |(\partial/\partial x)|\vec{B}(x)||$ inside the central region $(-L/2 < x < L/2)$ yielding

$$g(x) = \frac{1}{2} - \frac{\int_{-L/2}^{x} \mathrm{d}x\, |(\partial/\partial x)|\vec{B}(x)||}{\int_{-L/2}^{L/2} \mathrm{d}x\, |(\partial/\partial x)|\vec{B}(x)||}.$$

However, before we numerically investigate the ac ratchet transport properties, we exploit certain symmetries present in the system to simplify the expressions for the average net charge (2.9a) and spin currents (2.9b). For the magnetic field profile produced by a stripe magnetized in z-direction it is straightforward to show from equations (2.1) and (2.2) that the following symmetry relations hold true (see also figure 6):

$$B_x(-x) = -B_x(x), \qquad B_z(-x) = B_z(x),$$
$$A_y(-x) = -A_y(x), \qquad g(-x) = -g(x)\,.$$

Thus the Hamiltonian $\hat{\mathcal{H}} = \hat{\mathcal{H}}_0 + \hat{\mathcal{H}}_U$ is invariant under the action of the operator $\hat{\mathcal{P}} = -\mathrm{i}\hat{\mathcal{C}}\hat{R}_x\hat{R}_U\sigma_z$, where $\hat{\mathcal{C}}$ is the operator of complex conjugation, $\hat{R}_x$ inverses the x-coordinate, $\hat{R}_U$ changes the sign of the applied voltage ($\pm U_0 \to \mp U_0$) and σ_z is the Pauli spin operator. Due to $[\hat{\mathcal{H}}, \hat{\mathcal{P}}] = 0$, we are able to interrelate the transmission probabilities for both rocking situations as shown in appendix B. Taking the square of equation (B.3) and summing over the transversal modes $n \in L$ and $n' \in R$, we obtain the following relations between the spin-resolved transmission probabilities in the two rocking situations:

$$T_{\sigma,\sigma'}^{(\theta,\phi)}(E, \pm U_0) = T_{\sigma',\sigma}^{(\theta,-\phi+\pi)}(E, \mp U_0).$$

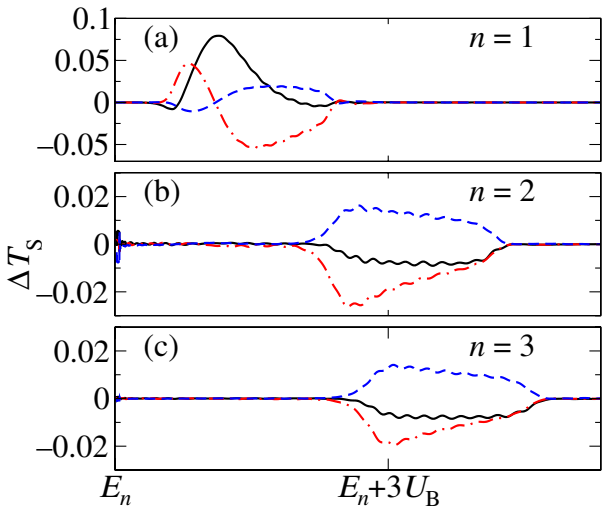

Figure 8. Averaged net spin transmission $\Delta T_{\mathrm{S}}(E; U_0)$ for spin polarization axes $\hat{x}$ (solid black line), $\hat{y}$ (dash-dotted red line) and $\hat{z}$ (dashed blue line) as a function of energy close to the lowest three transversal energy levels $E_n (n = 1, 2 \text{ and } 3)$ for an applied bias voltage of $U_0 = 0.1 U_{\mathrm{B}}$.

Here, the superscript labels the angles of the spin quantization axis on the Bloch sphere (see appendix B). Thus the ratchet charge current (2.9*a*) vanishes,

$$\langle I_{\mathrm{C}}(\varepsilon_{\mathrm{F}}, U_0)\rangle = 0,$$

and we can express the ratchet spin current (2.9*b*) through the transmission probabilities of a single rocking situation (e.g. $+U_0$):

$$\langle I_{\mathrm{S};x}(\varepsilon_{\mathrm{F}}, U_0)\rangle = \frac{1}{4\pi}\int_0^\infty \mathrm{d}E\, \Delta f(E; \varepsilon_{\mathrm{F}}, U_0)\Big[T_{+,+}(E, +U_0) - T_{-,-}(E, +U_0)\Big],$$

$$\langle I_{\mathrm{S};y/z}(\varepsilon_{\mathrm{F}}, U_0)\rangle = \frac{1}{4\pi}\int_0^\infty \mathrm{d}E\ \Delta f(E; \varepsilon_{\mathrm{F}}, U_0)\Big[T_{+,-}(E, +U_0) - T_{-,+}(E, +U_0)\Big].$$

Figure 8 shows the ratchet spin transmission $\Delta T_{\mathrm{S}}(E; U_0)$ at a finite applied voltage $U_0 = 0.1 U_{\mathrm{B}}$ for a wire of width $W = 120$ nm. This quantity is finite for energies where the dc transmission is spin polarized (see figure 7). Furthermore, the spin polarization of the ratchet spin transmission depends on the injection energy. This opens the possibility to tune it upon varying the Fermi energy. Comparing the ratchet spin transmission for $n = 1$ (figure 8 (a)) and $n = 2, 3$ (figures 8(b) and (c)), we observe that its magnitude is significantly lower in the case where more than one transversal mode is conducting. This behavior is due to the mixing of different transversal subbands due to $A_y(x)$. To quantify this effect, we introduce

$$\Delta T_{\mathrm{S,max}}(n) = \max_{E\in[E_n, E_{n+1}]}\left[\sqrt{\Delta T_{\mathrm{S};\hat{x}}(E)^2 + \Delta T_{\mathrm{S};\hat{y}}(E)^2 + \Delta T_{\mathrm{S};\hat{z}}(E)^2}\right],$$

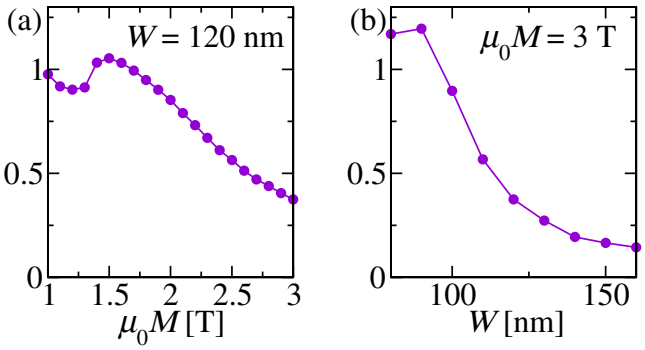

Figure 9. Ratio $\Delta T_{\mathrm{S,max}}(n=2)/\Delta T_{\mathrm{S,max}}(n=1)$ as a function of (a) the magnetization of the ferromagnetic stripe and (b) the wire width.

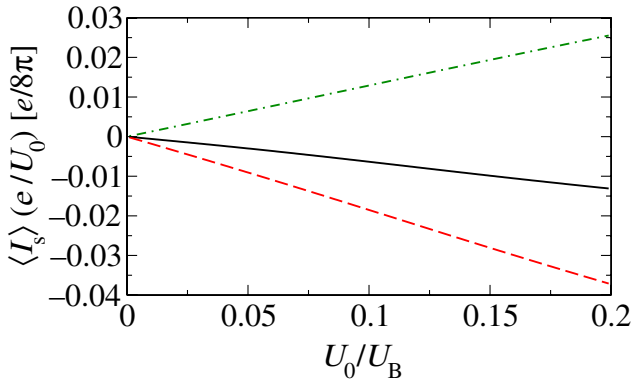

Figure 10. Ratchet spin conductance $\langle I_{\mathrm{S},\hat{u}}\rangle(e/U_0)$ as a function of bias voltage U_0 at $k_{\mathrm{B}}T=0$ and $\varepsilon_{\mathrm{F}}=E_3+3U_{\mathrm{B}}$ for the spin quantization directions $\hat{x}$ (black solid line), $\hat{y}$ (red dashed line) and $\hat{z}$ (green dash-dotted line).

as a measure for the rectification in each single transversal mode. Figure 9 shows that $\Delta T_{\mathrm{S,max}}(n=2)/\Delta T_{\mathrm{S,max}}(n=1)\approx 1$ for cases where the mixing due to $A_y(x)$ is small, i.e. for a narrow wire and/or small magnetic field. However, it decreases upon increasing $\mu_0 M$ and/or W. Note that for set-up A in the previous section, the magnetic field inside the quantum wire was one order of magnitude smaller than for set-up B here, thus yielding a comparable value $\Delta T_{\mathrm{S,max}}(n)$ for all subbands n.

As for set-up A, the ratchet spin conductance shown in figure 10 exhibits a linear dependence on the applied voltage. Thus, we presume that the rectification mechanism is the same as in set-up A, although the spin dynamics is much more intricate.

5. Conclusions and outlook

In the present work, we have shown that the coupling of the electron spin to the magnetic fringe fields of ferromagnetic stripes via the Zeeman interaction can be used to generate a spin ratchet effect in a coherent mesoscopic conductor subject to an adiabatic ac driving with finite bias.

The proposed devices exhibit the appealing property of creating a directed net spin current in the absence of an accompanying net charge transport. This key result has been demonstrated in numerical approaches for set-ups A and B, in the case of set-up B, also analytically based on symmetry properties of the system.

The generated spin current may be regarded as resulting from a rectification effect, however in a generalized sense: the direct analog of a charge current rectifier would be a system generating a directed spin current out of a conductor with alternating *spin-chemical* potentials in the left and right reservoir. Spin ratchets, such as the ones considered here, act differently as they convert an ac *electrical* bias into a net spin current.

From our analysis, we have identified the difference in the maximum values of the effective Zeeman potentials in the respective rocking situations as responsible for the creation of the spin current. It has been shown that this rectification effect is almost independent of the actual distribution of the electrostatic potential in the biased conductor. Furthermore, the fact that, for the systems considered here, the difference in the maximum values of the Zeeman potential is crucial for the spin currents, implies that the magnitude of the spin current cannot be systematically increased upon increasing the number of magnetic stripes, e.g. in a periodic arrangement of stripes. We have checked this also numerically by adding an increasing number of stripes.

In the preceding sections, we presented results when evaluating the spin current inside the right lead. However, as we noted both systems considered, set-ups A and B, are characterized by interesting symmetry properties. Those can now be used to directly extract the respective currents inside the left lead. If for set-up A the component A_x can be neglected, as it is appropriate for the parameters used in section 3, the combined Hamiltonian of the system and the leads has been proven to be invariant under the action of the symmetry operation $\hat{R}_x \hat{R}_y \hat{R}_U \sigma_z$, while for set-up B the Hamiltonian is invariant under the action of $\hat{R}_x \hat{R}_U \sigma_z$. These symmetry properties are reflected in equations (B.4) and (B.5) respectively, see appendix B. Both relations lead to the general relation

$$T'^{(\theta,\phi+\pi)}_{\sigma,\sigma'}(E, \mp U_0) = T^{(\theta,\phi)}_{\sigma,\sigma'}(E, \pm U_0),$$

between the transmission probabilities in the two rocking situations. This relation allows for the following interpretation. If the transmitted electrons are spin-polarized in one of the two rocking situations with direction of the polarization vector given by the angles (θ, ϕ) on the Bloch sphere, then in the other rocking situation the spin polarization vector of the output current (in the other lead) will be rotated around the z-axis by π and thus points to $(\theta, \phi + \pi)$. This property is a direct consequence of the lacking conservation of the spin eigenstates inside the wire.

The physics of semiconducting materials characterized by a large g^* factor is dominated by the presence of magnetic impurities, e.g. diluted magnetic semiconductors [34]. Therefore, in order to exploit the expected stronger rectification effect, we have to take elastic scattering off impurities into account. In particular, we plan to study how additional disorder alters the spin ratchet effects.

Finally, since the heuristic model used for the distribution of the electrostatic potential in the conductor is convenient but not fully satisfactory, it would be desirable to calculate the charge density and the respective electrostatic potential inside the wire self-consistently. Work in this direction is in progress.

Acknowledgments

We acknowledge discussions with and computational support by Michael Wimmer. This research has been supported by the Deutsche Forschungsgemeinschaft within the cooperative research center SFB 689 'Spin phenomena in reduced dimensions' and the research training group GRK 638. MS acknowledges support through the Studienstiftung des Deutschen Volkes.

Appendix A. Calculation of the spin current in the Landauer–Büttiker formalism

In this appendix, we present a derivation of the expressions for spin current in the leads of a multiterminal coherent conductor within the framework of the Landauer–Büttiker theory [45]. To this end, we consider N non-ferromagnetic contacts, injecting spin-unpolarized current into the leads. For convenience, we use a local coordinate system for the lead under investigation, where x is the coordinate along the lead in the direction of charge propagation due to an applied bias in linear response and y is the transverse coordinate. Then the eigenfunctions inside a lead are given by

$$\Phi^{\pm}_{E,n\sigma}(x,y) = \frac{1}{\sqrt{k_x(E)}} \mathrm{e}^{\pm \mathrm{i}k_x(E)x} \chi_n(y)\Sigma(\sigma), \tag{A.1}$$

where the $\chi_n(y)$ are the transverse eigenfunctions of the lead with the transversal eigenenergy E_n and $\Sigma(\sigma)$ is the spin eigenfunction. The superscript $\pm$ of Φ refers to the direction of motion in $\pm x$-direction with the wavevector $k_x = \sqrt{2m^*(E-E_n)}/\hbar$. For the derivation we use the scattering approach, where the amplitudes of the states inside the leads are related via the scattering matrix $\mathbf{S}(E)$, determined by the Hamiltonian of the coherent conductor. Inside lead q a given scattering state

$$\varphi^q_E(x,y) = \sum_{(n\sigma)\in q} \left(a^q{}_{n\sigma}(E)\Phi^+_{E,n\sigma}(x,y) + b^q{}_{n\sigma}(E)\Phi^-_{E,n\sigma}(x,y) \right),$$

($\sigma = \pm$), consists of incoming states Φ^+ entering the coherent conductor from contact q and outgoing states Φ^- leaving the coherent conductor into contact q. The amplitudes of incoming $a^j_{n\sigma}$ and outgoing waves $b^i_{n'\sigma'}$ are related via the equation

$$b^i_{n'\sigma'}(E) = \sum_{j=1}^{N} \sum_{n\in j} \sum_{\sigma=\pm 1} S^{i,j}_{n'\sigma',n\sigma}(E) a^j_{n\sigma}(E), \tag{A.2}$$

where the scattering matrix $\mathbf{S}(E)$ has the following structure for an N terminal system:

$$\mathbf{S}(E) = \begin{pmatrix} \mathbf{r}^{1,1}(E) & \mathbf{t}^{1,2}(E) & \cdots & \mathbf{t}^{1,N}(E) \\ \mathbf{t}^{2,1}(E) & \mathbf{r}^{2,2}(E) & \cdots & \mathbf{t}^{2,N}(E) \\ \vdots & \vdots & \ddots & \vdots \\ \mathbf{t}^{N,1}(E) & \mathbf{t}^{N,2}(E) & \cdots & \mathbf{r}^{N,N}(E) \end{pmatrix}.$$

Here the sub-matrix $\mathbf{r}^{j,j}(E)$ is a square matrix of dimensionality $M^j(E)$, corresponding to the number of open channels at energy E in lead j (already including the spin degree of freedom), which is connected to a reservoir with chemical potential μ_j. The matrix $\mathbf{r}^{j,j}(E)$ contains the scattering amplitudes of incoming channels of lead j being reflected back into outgoing channels of the same lead. The sub-matrix $\mathbf{t}^{i,j}(E)$ is a $M^i(E) \times M^j(E)$ matrix that contains the

scattering amplitudes for transmission between incoming channels from lead j and outgoing channels of lead i.

The wavefunction of the scattering state inside lead i, where only the incoming channel $(n\sigma) \in j$ is populated ($a^{j'}_{n'\sigma'} = \delta_{j',j}\delta_{n',n}\delta_{\sigma',\sigma}$), reads for $j = i$:

$$\varphi^{i}_{E,n\sigma}(x, y) = \Phi^{+}_{E,n\sigma}(x, y) + \sum_{(n'\sigma')\in i} r^{i,i}_{n'\sigma',n\sigma}(E)\Phi^{-}_{E,n'\sigma'}(x, y), \tag{A.3}$$

and, correspondingly, for $j \neq i$

$$\varphi^{i}_{E,n\sigma}(x, y) = \sum_{(n'\sigma')\in i} t^{i,j}_{n'\sigma',n\sigma}(E)\Phi^{-}_{E,n'\sigma'}(x, y). \tag{A.4}$$

For a wavefunction $\Psi(x, y)$ the spin current $I^{\Psi}_{S}(x)$ passing a cross section ($x = \text{const.}$) of a lead is given by:

$$I^{\Psi}_{S}(x) = \int \mathrm{d}y\, \Psi^{*}(x, y)\hat{J}_{S}\Psi(x, y). \tag{A.5}$$

Here, we use the most common definition of the spin current operator [36], which with respect to an arbitrary quantization axis $\hat{u}$ takes the following form inside the leads:

$$\hat{J}_{S} = \frac{\hbar}{2}\frac{\hbar}{2m^{*}i}(\vec{\sigma}\cdot\hat{u})\left(\frac{\overrightarrow{\partial}}{\partial x} - \frac{\overleftarrow{\partial}}{\partial x}\right).$$

The partial derivatives act on the expressions to their right/left respectively (indicated by the arrows). For the scattering state (A.3) we then obtain for the spin current (A.5) inside lead i

$$I^{j=i}_{S;E,n\sigma}(x \in i) = \frac{\hbar^2}{2m^{*}}\left[\sigma - \sum_{(n'\sigma')\in i}\sigma' \left|r^{i,i}_{n'\sigma',n\sigma}(E)\right|^2\right],$$

where $(n\sigma \in j,\ j = i)$. For the scattering state (A.4) we find the corresponding expression $(n\sigma \in j,\ j \neq i)$

$$I^{j\neq i}_{S;E,n\sigma}(x \in i) = -\frac{\hbar^2}{2m^{*}}\sum_{(n'\sigma')\in i}\sigma' \left|t^{i,j}_{n'\sigma',n\sigma}(E)\right|^2.$$

Since every channel is populated according to the Fermi–Dirac distribution $f(E;\mu_q)$ of the respective contact q, the total spin current in lead i then reads

$$\begin{aligned} I_{S}(x \in i) &= \frac{m^{*}}{2\pi\hbar^2}\int_0^{\infty}\mathrm{d}E\left[\sum_{j=1}^{N}\sum_{(n\sigma)\in j} f(E;\mu_j)I^{j}_{S;E,n\sigma}(x \in i)\right] \\ &= \frac{-1}{4\pi}\int_0^{\infty}\mathrm{d}E\left[f(E;\mu_i)R^{i,i}_{S}(E) + \sum_{q\neq i} f(E;\mu_q)T^{i,q}_{S}(E)\right], \end{aligned} \tag{A.6}$$

where

$$T^{i,q}_{S}(E) = \sum_{\sigma'=\pm}\left(T^{i,q}_{+,\sigma'} - T^{i,q}_{-,\sigma'}\right), \qquad R^{i,i}_{S}(E) = \sum_{\sigma'=\pm}\left(R^{i,i}_{+,\sigma'} - R^{i,i}_{-,\sigma'}\right),$$

and

$$T^{i,q}_{\sigma,\sigma'}(E) = \sum_{n\in i}\sum_{n'\in q}\left|t^{i,q}_{n\sigma,n'\sigma'}(E)\right|^2, \tag{A.7}$$

$$R^{i,i}_{\sigma,\sigma'}(E) = \sum_{n\in i}\sum_{n'\in i}\left|r^{i,i}_{n\sigma,n'\sigma'}(E)\right|^2. \tag{A.8}$$

Since $\mathbf{S}(E)$ is unitary, the following relation holds true:

$$\sum_{(n'\sigma')\in i}\left|r^{i,i}_{n\sigma,n'\sigma'}(E)\right|^2 + \sum_{q\neq i}\sum_{(n''\sigma'')\in q}\left|t^{i,q}_{n\sigma,n''\sigma''}(E)\right|^2 = 1.$$

Then it is straightforward to show that

$$R^{i,i}_{\mathrm{S}}(E) + \sum_{q\neq i} T^{i,q}_{\mathrm{S}}(E) = 0,$$

In view of equation (A.6), we eventually find for the spin current in lead i

$$I_{\mathrm{S}}(x\in i) = \frac{1}{4\pi}\int_0^\infty \mathrm{d}E \sum_{q\neq i}\left[f(E;\mu_i) - f(E;\mu_q)\right] T^{i,q}_{\mathrm{S}}(E). \tag{A.9}$$

Although equilibrium spin currents can locally exist in systems with SO interactions as shown for 2DEGs [46] and in mesoscopic systems [47], equation (A.9) clearly shows that in thermal equilibrium ($\mu_j = \mu$) the spin current inside leads without SO interactions and magnetic fields vanishes. This absence of equilibrium spin currents in the leads has been shown for systems with preserved time-reversal symmetry [48]. However, here we show that it is more generally valid for any coherent conductor, since we did not make any assumptions about symmetries of the scattering region in the course of the derivation.

We note that the relation (5) derived by Pareek [49] that allows for equilibrium spin currents, has to be regarded as incorrect, arising from an improper treatment of the back-reflection, missing the term

$$\frac{1}{4\pi}\int_0^\infty \mathrm{d}E\ f(E;\mu_i) 2\left(R^{i,i}_{-,+}(E) - R^{i,i}_{+,-}(E)\right), \tag{A.10}$$

in comparison with equation (A.9). This issue has been addressed by Nikolic *et al* [50]. However, their argumentation that the term (A.10) has only to be included in equilibrium, i.e. for energies up to the lowest chemical potential of the N terminals, seems questionable. If the spin current is evaluated in a lead connected to a reservoir k with $\mu_k > \mu_l$ (μ_l being the lowest chemical potential of any of the N reservoirs), the full expression (A.9) has to be used. Furthermore, a simplified version of equation (A.9),

$$I_{\mathrm{S}} = \frac{1}{4\pi}\sum_{q\neq i}(\mu_i - \mu_q) T^{i,q}_{\mathrm{S}},$$

where transport at zero temperature and energy-independent transmission probabilities were considered, has been used in recent publications on the mesoscopic spin Hall effect [51].

Appendix B. Derivation of symmetry relations for spin-dependent Landauer transport at finite bias

Here, we derive symmetry relations for a two terminal set-up as used in this paper. We generalize related expressions from [52] to finite bias and arbitrary spin quantization axis.

If the Hamiltonian of the total system of scattering region and leads is invariant under certain symmetry operations $\hat{\mathcal{P}}$, we can relate the elements of the scattering matrix even in different rocking situations. As an example, we derive the symmetry relations stemming from the symmetry operator $\hat{\mathcal{P}} = -\mathrm{i}\hat{\mathcal{C}}\hat{R}_x\hat{R}_U\sigma_z$, where $\hat{\mathcal{C}}$ is the operator of complex conjugation, $\hat{R}_x$ inverts the x-coordinate, $\hat{R}_U$ changes the sign of the applied voltage ($\pm U_0 \to \mp U_0$) and σ_z is the Pauli spin operator.

Generalizing equation (A.1) of appendix A the eigenfunctions inside the leads are given by

$$\Phi^{\pm,(\theta,\phi)}_{E,n\sigma}(x,y) = \frac{1}{\sqrt{k_x(E)}}\mathrm{e}^{\pm\mathrm{i}k_x(E)x}\chi_n(y)\Sigma_{(\theta,\phi)}(\sigma), \tag{B.1}$$

with the spin eigenstates

$$\Sigma_{(\theta,\phi)}(+) = \begin{pmatrix}\cos\frac{\theta}{2}\mathrm{e}^{-\mathrm{i}\phi/2}\\ \sin\frac{\theta}{2}\mathrm{e}^{\mathrm{i}\phi/2}\end{pmatrix},\ \Sigma_{(\theta,\phi)}(-) = \begin{pmatrix}-\sin\frac{\theta}{2}\mathrm{e}^{-\mathrm{i}\phi/2}\\ \cos\frac{\theta}{2}\mathrm{e}^{\mathrm{i}\phi/2}\end{pmatrix},$$

defined with respect to the quantization axis

$$\hat{u} = \begin{pmatrix}\sin\theta\cos\phi\\ \sin\theta\sin\phi\\ \cos\theta\end{pmatrix}.$$

The effect of $\hat{\mathcal{P}}$ on the eigenstates (B.1) is to change an incoming state in the left lead (L) in one rocking situation into an outgoing state of the right lead (R) in the other rocking situation and vice versa. Furthermore, the position of the spin on the Bloch sphere is changed from (θ, ϕ) into $(\theta, -\phi+\pi)$, and the amplitude of the state is complex conjugated.

On the other hand, the action of $\hat{\mathcal{P}}$ cannot change the scattering-matrix, since the Hamiltonian is invariant under the action of $\hat{\mathcal{P}}$. Therefore, the following relation holds true:

$$a^{(\theta,-\phi+\pi)*}_{\bar{n}\sigma}(E,\mp U_0) = \sum_{n'\in(\mathrm{L}\cup\mathrm{R})}\sum_{\sigma'=\pm1} S^{(\theta,\phi)}_{n\sigma,n'\sigma'}(E,\pm U_0)b^{(\theta,-\phi+\pi)*}_{\bar{n}'\sigma'}(E,\mp U_0). \tag{B.2}$$

Here, the mode index $\bar{n}$ is related to mode n of the opposite lead by means of the symmetry transformation. Comparing equation (B.2) with the inverse of equation (A.2),

$$a^{(\theta,-\phi+\pi)}_{n\sigma}(E,\mp U_0) = \sum_{n'\in(\mathrm{L}\cup\mathrm{R})}\sum_{\sigma'=\pm1}\left[S^{(\theta,-\phi+\pi)}\right]^{-1}_{n\sigma,n'\sigma'}(E,\mp U_0)b^{(\theta,-\phi+\pi)}_{n'\sigma'}(E,\mp U_0),$$

and using the unitarity of the scattering matrix, $\mathbf{S}^{-1} = \mathbf{S}^\dagger = (\mathbf{S}^*)^\mathrm{t}$, we find the symmetry relation for the scattering amplitudes

$$S^{(\theta,-\phi+\pi)}_{n\sigma,n'\sigma'}(E,\mp U_0) = S^{(\theta,\phi)}_{\bar{n}'\sigma',\bar{n}\sigma}(E,\pm U_0). \tag{B.3}$$

Similar relations can be obtained for any other symmetry operator that commutes with the Hamiltonian $\hat{\mathcal{H}}$. For the other two operators used in this paper, $\hat{R}_x\hat{R}_U\sigma_z$ and $\hat{R}_x\hat{R}_y\hat{R}_U\sigma_z$, the above procedure can be applied accordingly. It yields

$$S^{(\theta,\phi+\pi)}_{n\sigma,n'\sigma'}(E,\mp U_0) = S^{(\theta,\phi)}_{\bar{n}\sigma,\bar{n}'\sigma'}(E,\pm U_0) \tag{B.4}$$

for $[\hat{\mathcal{H}},\,\hat{R}_x\hat{R}_U\sigma_z]=0$ and

$$S^{(\theta,\phi+\pi)}_{n\sigma,n'\sigma'}(E,\mp U_0) = p_n p_{n'} S^{(\theta,\phi)}_{\bar{n}\sigma,\bar{n}'\sigma'}(E,\pm U_0) \tag{B.5}$$

for $[\hat{\mathcal{H}},\,\hat{R}_x\hat{R}_y\hat{R}_U\sigma_z]=0$, where $p_n=(-1)^{n-1}$ is the parity of the eigenfunction $\chi_n(y)$ in equation (B.1).

References

[1] Datta S and Das B 1990 *Appl. Phys. Lett.* **56** 665
[2] Rashba E I 1960 *Sov. Phys. Solid State* **2** 1109
[3] Schmidt G, Ferrand D, Molenkamp L W, Filip A T and van Wess B J 2000 *Phys. Rev.* B **62** R4790
[4] Fiederling R, Keim M, Reuscher G, Ossau W, Schmidt G, Waag A and Molenkamp L W 1999 *Nature* **402** 787
[5] Ohno Y, Young D K, Beschoten B, Matsukura F, Ohno H and Awschalom D D 1999 *Nature* **402** 790
[6] Ganichev S D, Danilov S N, Eroms J, Wegscheider W, Weiss D, Prettl W and Ivchenko E L 2001 *Phys. Rev. Lett.* **86** 4358
[7] Murakami S, Nagaosa N and Zhang S C 2003 *Science* **301** 1348
[8] Sinova J, Culcer D, Niu Q, Sinitsyn N A, Jungwirth T and MacDonald A H 2004 *Phys. Rev. Lett.* **92** 126603
[9] Kato Y K, Mayer R C, Gossard A C and Awschalom D D 2004 *Science* **306** 1910
[10] Wunderlich J, Kaestner B, Sinova J and Jungwirth T 2005 *Phys. Rev. Lett.* **94** 47204
[11] Sih V, Myers R C, Kato Y K, Lau W H, Gossard A C and Awschalom D D 2005 *Nat. Phys.* **1** 31
[12] Valenzuela S O and Tinkham M 2006 *Nature* **442** 176
[13] Kimura T, Otani Y, Sato T, Takahashi S and Maekawa S 2007 *Phys. Rev. Lett.* **98** 156601
Kimura T, Otani Y, Sato T, Takahashi S and Maekawa S 2007 *Phys. Rev. Lett.* **98** 249901 (erratum)
[14] Sharma P and Chamon C 2001 *Phys. Rev. Lett.* **87** 96401
[15] Mucciolo E R, Chamon C and Marcus C M 2002 *Phys. Rev. Lett.* **89** 146802
[16] Governale M, Taddei F and Fazio R 2003 *Phys. Rev.* B **68** 155324
[17] Scheid M, Pfund A, Bercioux D and Richter K 2007 *Phys. Rev.* B **76** 195303 (*Preprint* cond-mat/0601118)
[18] Scheid M, Wimmer M, Bercioux D and Richter K 2006 *Phys. Status Solidi* c **3** 4235
[19] Brouwer P W 1998 *Phys. Rev.* B **58** R10135
[20] Watson S K, Potok R M, Marcus C M and Umansky V 2003 *Phys. Rev. Lett.* **91** 258301
[21] Reimann P 2002 *Phys. Rep.* **361** 57
[22] Reimann P, Grifoni M and Hänggi P 1997 *Phys. Rev. Lett.* **79** 10
[23] Linke H, Humphrey T E, Löfgren A, Sushkov A O, Newbury R, Taylor R P and Omling P 1999 *Science* **268** 2314
[24] Linke H, Humphrey T R, Lindelof P R, Löfgren A, Newbury R, Omling P, Sushkov A O, Taylor R P and Xu H 2002 *Appl. Phys.* A **75** 237
[25] Braunecker B, Feldman D E and Li F 2007 *Phys. Rev.* B **76** 085119
[26] Matulis A, Peeters F M and Vasilopoulos P 1994 *Phys. Rev. Lett.* **72** 1518
[27] Ye P D, Weiss D, Gerhardts R R, Seeger M, Klitzing K von, Eberl K and Nickel H 1995 *Phys. Rev. Lett.* **74** 3013
[28] Kubrak V, Rahman F, Gallagher B L, Main P C, Henini M, Marrows C H and Howson M A 1999 *Appl. Phys. Lett.* **74** 2507

[29] Kubrak V, Neumann A C, Gallagher B L, Main P C, Henini M, Marrows C H and Howson M A 2000 *Physica* E **6** 755
[30] Jackson J D 1999 *Classical Electrodynamics* (New York: Wiley)
[31] Zhai F and Xu H Q 2006 *Appl. Phys. Lett.* **88** 032502
[32] Lu M, Zhang L, Jin Y and Yan X 2002 *Eur. Phys. J.* B **27** 565
[33] Slobodskyy A, Gould C, Slobodskyy T, Becker C R, Schmidt G and Molenkamp L W 2003 *Phys. Rev. Lett.* **90** 246601
[34] Furdyna J K 1988 *J. Appl. Phys.* **64** R29
[35] Madelung O 2003 *Semiconductors: Data Handbook* (Berlin: Springer)
[36] Rashba E I 2005 *J. Supercond.* **18** 137
[37] Waintal X, Myers E B, Brouwer P W and Ralph D C 2000 *Phys. Rev.* B **62** 12317
[38] Shi J, Zhang P, Xiao D and Niu Q 2006 *Phys. Rev. Lett.* **96** 76604
[39] Büttiker M 1993 *J. Phys.: Condens. Matter* **5** 9361
[40] Christen T and Büttiker M 1996 *Europhys. Lett.* **35** 523
[41] Xu H 1993 *Phys. Rev.* B **47** 15630
[42] Lassl A, Schlagheck P and Richter K 2007 *Phys. Rev.* B **75** 045346
[43] Sablikov V A, Borisov V I and Chmil' A I 2005 *JETP Lett.* **81** 75
[44] Governale M and Boese D 2000 *Appl. Phys. Lett.* **77** 3215
[45] Büttiker M, Imry Y, Landauer R and Pinhas S 1985 *Phys. Rev.* B **31** 6207
[46] Rashba E I 2003 *Phys. Rev.* B **68** 241315
[47] Nikolic B K, Zârbo L P and Souma S 2006 *Phys. Rev.* B **73** 075303
[48] Kiselev A A and Kim K W 2005 *Phys. Rev.* B **71** 153315
[49] Pareek T P 2004 *Phys. Rev. Lett.* **92** 076601
[50] Nikolic B K, Zârbo L P and Souma S 2005 *Phys. Rev.* B **72** 075361
[51] Hankiewicz E M, Molenkamp L W, Jungwirth T and Sinova J 2004 *Phys. Rev.* B **70** 241301
Ren W, Qiao Z, Wang Q Sun and Guo H 2006 *Phys. Rev. Lett.* **97** 066603
Bardarson J H, Adagideli I and Jacquod P 2007 *Phys. Rev. Lett.* **98** 196601
[52] Zhai F and Xu H Q 2005 *Phys. Rev. Lett.* **94** 246601